



The Stellar Merger Scenario for Black Holes in the Pair-instability Gap

M. Renzo^{1,2} , M. Cantiello^{1,3} , B. D. Metzger^{1,2} , and Y.-F. Jiang (姜燕飞)¹

¹Center for Computational Astrophysics, Flatiron Institute, New York, NY 10010, USA

²Department of Physics, Columbia University, New York, NY 10027, USA

³Department of Astrophysical Sciences, Princeton University, Princeton, NJ 08544, USA

Received 2020 October 1; revised 2020 October 19; accepted 2020 October 31; published 2020 November 23

Abstract

The recent detection of GW190521 stimulated ideas on how to populate the predicted black hole (BH) pair-instability (PI) mass gap. One proposal is the dynamical merger of two stars below the PI regime forming a star with a small core and an oversized envelope. We outline the main challenges this scenario faces to form one BH in the gap. In particular, the core needs to avoid growing during the merger, and the merger product needs to retain enough mass, including in the subsequent evolution, and at core collapse (CC). We explore this scenario with detailed stellar evolution calculations, starting with ad hoc initial conditions enforcing no core growth during the merger. We find that these massive merger products are likely to be helium-rich and spend most of their remaining lifetime within regions of instabilities in the Hertzsprung–Russell diagram, such as luminous blue variable eruptions. An energetic estimate of the amount of mass loss neglecting the back reaction of the star suggests that the total amount of mass that can be removed at low metallicity is $\lesssim 1 M_{\odot}$. This is small enough that at CC our models are retaining sufficient mass to form BHs in the PI gap similar to the recent ones detected by LIGO/Virgo. However, mass loss at the time of merger, the resulting core structure, and the mass loss at CC still need to be quantified for these models to confirm the viability of this scenario.

Unified Astronomy Thesaurus concepts: Massive stars (732); Black holes (162); Luminous blue variable stars (944); Stellar mergers (2157)

1. Introduction

The existence of a mass gap where pair-instability (PI) supernovae (SNe, e.g., Barkat et al. 1967) prevent the formation of black holes (BH) is a robust prediction of stellar evolution theory (e.g., Woosley et al. 2002; Woosley 2017; Farmer et al. 2019; Leung et al. 2019; Marchant et al. 2019; Marchant & Moriya 2020; Renzo et al. 2020b, 2020a). However, the detection of GW190521 (Abbott et al. 2020a, 2020b) is challenging this prediction. For this merger event *both* BH masses, $^{+21}_{-14} 85 M_{\odot}$ and $^{+17}_{-18} 66 M_{\odot}$, are in the PI mass gap situated roughly between $\sim 45 M_{\odot}$ and $\sim 130 M_{\odot}$ (e.g., Woosley et al. 2002; Farmer et al. 2019, 2020).

These BHs might not be the direct remnants of stars, but rather the product of second-generation BH mergers in a (nuclear) cluster (e.g., Perna et al. 2019; Fragione et al. 2020; Kremer et al. 2020; Mapelli et al. 2020; Rodriguez et al. 2020) or active galactic nucleus disk (e.g., McKernan et al. 2012, 2014; Bartos et al. 2017; Stone et al. 2017; Fragione et al. 2019), of accretion from gas clouds (e.g., Roupas & Kazanas 2019; Safarzadeh & Haiman 2020), or possibly primordial BHs (De Luca et al. 2020).

Many possible stellar explanations for the formation of BHs in the gap have also been proposed. These include reduction by $\gtrsim 2\sigma$ of the $^{12}\text{C}(\alpha, \gamma)^{16}\text{O}$ reaction rate (Farmer et al. 2020; Belczynski 2020), modifications to the standard model (Croon et al. 2020a, 2020b; Sakstein et al. 2020), and Population III stars (Farrell et al. 2020; Kinugawa et al. 2020). BHs accreting in isolated binaries do not contribute significantly to populating the PI mass gap (van Son et al. 2020).

We focus on one particular scenario proposed by Spera et al. (2019) and Di Carlo et al. (2019, 2020a, 2020b): the formation

of BHs in the PI mass gap via stellar mergers in a dynamical environment. Section 2 summarizes this “stellar merger” scenario and its challenges. We then construct stellar models for the merger product in Section 3, and evolve them. Section 4 shows how evolutionary processes can lead to continuum-driven mass loss that is not considered in rapid population-synthesis models underlying *N*-body calculations. We estimate the amount of mass loss, and conclude that by itself it might not change the scenario appreciably.

2. The Stellar Merger Scenario

Di Carlo et al. (2020b) presented a detailed example of this scenario (see their Figure 7), where the dynamically driven merger happens at the end of the main sequence of a $\sim 58 M_{\odot}$ star. At this point the total mass of a $\sim 42 M_{\odot}$ star is added to the envelope *without* modifying the core. Thus, the merger product has a small core and an oversized envelope, and reaches core collapse (CC) with a total mass of $\sim 99 M_{\odot}$. At this point, Di Carlo et al. (2019, 2020a, 2020b) assumed a direct collapse to BH, without mass ejection but accounting for a reduction in gravitational mass due to neutrino losses.

In order to form a coalescing binary BH with masses in the PI mass gap, this scenario faces the following four challenges.

2.1. The Merger Challenge: Mass Loss, Core Size, and Rotation

The first challenge is retaining sufficient mass during the stellar collision and forming a post-merger structure without modifying the core.

Lombardi et al. (2002) performed SPH simulations of low-mass stellar collisions and found that their models lose 1%–7% of the total mass during the mergers. Glebbeek et al. (2013) computed SPH simulations of head-on collisions of massive

⁴ However, see also Fishbach & Holz 2020 for a population-informed re-analysis reconciling the masses with stellar evolution predictions.

stars. For their most massive objects ($40 M_{\odot} + 40 M_{\odot}$) they found a mass loss corresponding to 6%–8% of the total mass. However, these models neglect the effects of radiation transport, which could have an important role for the mass budget in the merger of very luminous stars. Including radiation effects would likely increase the mass-loss rate during the merger, because the radiation-pressure-dominated envelope of very massive stars are loosely bound and easily stripped.

A back-of-the-envelope estimate of the amount of mass loss can be obtained considering that the energy available to drive mass loss is (a fraction of) the relative kinetic energy of the two incoming stars

$$E_{\text{kin}} \sim \frac{1}{2} \frac{M_1 M_2}{M_1 + M_2} v_{\sigma}^2 \lesssim 10^{46} \text{ erg} \ll E_{\text{bind}}, \quad (1)$$

where we use the aforementioned masses and assume $v_{\sigma} \lesssim 10 \text{ km s}^{-1}$ as the velocity dispersion of the cluster, and E_{bind} is the typical binding energy of the stars. Our pre-merger models (see Section 3) only have $\lesssim 10^{-3} M_{\odot}$ with binding energy lower than 10^{46} erg. This suggests that mergers resulting in small mass loss might be possible, however, using instead the escape velocity from the star in E_{kin} would result in a significantly higher mass loss. Our estimate neglects the stellar reaction to the energy injection during the merger process.

A second challenge is maintaining the core mass below the pulsational pair-instability (PPI) regime. The result of a stellar collision is often approximated using entropy sorting (e.g., Lombardi et al. 2002; Gaburov et al. 2008): this effectively would result in merging the cores of both stars and increasing the resulting core mass. Dynamical interaction might also pair stars in tight binaries merging later in a common envelope event. Merger simulations involving one evolved and one unevolved star are often invoked to explain the progenitor of SN1987A (e.g., Podsiadlowski 1992; Menon & Heger 2017), and in this case mixing into the core decreasing its mass has been proposed.

Merger products are also expected to be fast rotators (e.g., de Mink et al. 2013), although Schneider et al. (2019) found internal redistribution of angular momentum preventing fast surface rotation. If a large amount of angular momentum is transported in the core, rotational mixing (e.g., Maeder & Meynet 2000) might increase the core mass pushing the star into the PPI regime.

We do not investigate how realistic is the merger structure proposed by Spera et al. (2019) and Di Carlo et al. (2020a, 2020b). Following these studies, we assume that no mass is lost during the merger process and we do not consider the effects of rotation.

2.2. The Evolution Challenge: Winds and Envelope Instabilities

After the merger, low metallicity is necessary to prevent large line-driven wind mass loss (e.g., Farrell et al. 2020; Kinugawa et al. 2020), or it needs to be artificially suppressed (Belczynski et al. 2020). The angular momentum distribution might also lead to centrifugally driven mass loss (Langer 1998; Heger et al. 2000; Zhao & Fuller 2020).

Other modes of mass loss such as continuum-driven winds and/or luminous blue variable (LBV) eruptions are typically

not considered. However, merger products are prime candidates to explain LBV stars (e.g., Justham et al. 2014; Aghakhanloo et al. 2017) because of their increased luminosity, non-standard internal structure, and possible He-enrichment. He opacity is thought to have a key role in driving eruptive mass loss (Jiang et al. 2018), which could make this type of mass loss relatively metallicity-independent.

Our simple models presented in Section 4 address this problem mainly at metallicity $Z = 2 \times 10^{-4}$ (e.g., Di Carlo et al. 2020a); however, this challenge is expected to become progressively harder at higher Z , because of the increasing opacity in the stellar envelope.

2.3. The Collapse Challenge: Mass Loss at BH Formation

At BH formation, $\sim 10^{53}$ erg of neutrino emission is expected to suddenly decrease the gravitational mass of the collapsing core. This in turns creates a shock propagating thorough the envelope that can unbind the outer layers (e.g., Nadezhin 1980; Lovegrove & Woosley 2013; Fernández et al. 2018). While in the calculations of Di Carlo et al. (2020b) the BH mass accounts for the neutrino losses, the impact on the envelope mass loss was not investigated.

If the envelope is not lost at CC, it still could retain enough angular momentum to allow for the formation of an accretion disk. This could result in (ultra)-long gamma-ray bursts (e.g., Perna et al. 2018) and the delayed ejection of a significant fraction of the envelope. Even in the absence of net rotation, the fallback of large convective cells in the envelope could also drive the formation of disks and ultimately produce large amounts of mass loss through jets (Quataert et al. 2019).

2.4. The Gravitational-wave Challenge: Dynamical Pairing

If the previous challenges can be overcome, this scenario allows for the formation of single BHs in the gap. Dynamical interactions are then required to pair two of these BHs together in a tight orbit. Because of their large masses, these BHs are efficient at finding companions to merge with, with typical delay-time distribution of order tens of Myr. Di Carlo et al. (2020a) found a significant fraction of the merger rate from cluster dynamics to involve one BH from the stellar merger scenario (see also Spera et al. 2019; Di Carlo et al. 2019, 2020b; Kremer et al. 2020). However, to explain the masses in GW190521, both BHs should have formed via such evolutionary path.

3. Constructing a Merger Model

We use Modules for Experiments in Stellar Astrophysics (MESA; revision 12778; Paxton et al. 2011, 2013, 2015, 2018, 2019) to construct a post-merger structure. We do not compute the dynamical phase of the merger, but rather construct an ad hoc post-merger structure starting from the pre-merger stars. Details of the numerical implementation, together with the microphysics inputs, are given in Appendix.

3.1. Initial Chemical Composition

Following Di Carlo et al. (2020b), we assume that the merger happens at the end of the main sequence of a $M_1 = 58 M_{\odot}$ star at $Z = 2 \times 10^{-4}$. Using Brott et al. (2011) overshooting, its main-sequence lifetime is $\tau_{\text{MS}} = 4.15 \text{ Myr}$,

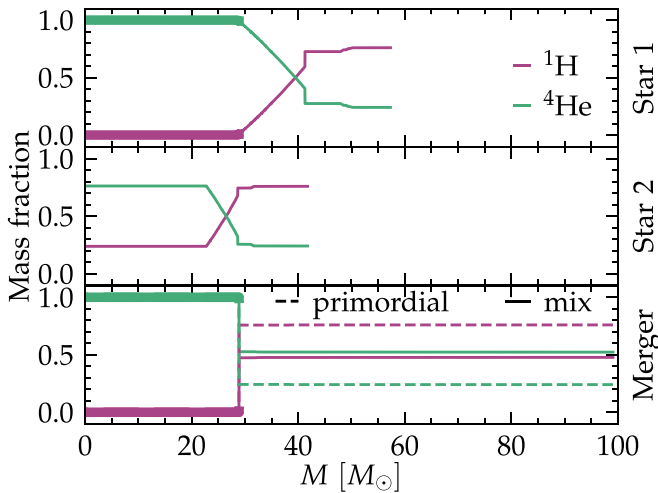


Figure 1. H and He profiles of the two pre-merger stars (top and middle panels) and of the merger products (bottom panel). In the bottom panel, solid (dashed) lines indicate the envelope composition for the “mix” (“primordial”) model. Both models have by construction the same core structure of the most massive star pre-merger (thicker lines). The least massive Star 2 is too young to have a well-defined He core.

and the corresponding Helium (He) core mass is $\sim 29 M_{\odot}$. This value is below the limit for any kind of PI pulse (Renzo et al. 2020a). We evolve up to $\tau_{\text{MS}} M_2 = 42 M_{\odot}$ star with the same setup. Very massive stars have comparable lifetimes, and by this time, the second star has a central He abundance $X_c(^4\text{He}) = 0.76$ extending out to mass coordinate $\sim 25 M_{\odot}$ (see the middle panel of Figure 1). The Kelvin–Helmholtz timescale of these stars is of order 10^4 years. After the merger, a relaxation phase of comparable duration is expected (although both the luminosity and radius are likely to be higher right after the merger; see, e.g., Schneider et al. 2019).

To construct the merger product, we first relax (e.g., Morozova et al. 2015; Vigna-Gómez et al. 2019) the most massive star model to $M_{\text{tot}} = M_1 + M_2 - \Delta M_{\text{wind}}$, where the mass lost to winds ΔM_{wind} is only $\sim 0.9 M_{\odot}$ using the Vink et al. (2001) algorithm. The mass relaxation procedure does not account for the release of gravitational or internal energy from the newly accreted mass. Then, we relax the chemical composition of the merger.

The top and middle panels in Figure 1 show the pre-merger composition of the two stars, and the bottom panel shows two different merger products. For both, we enforce the hypothesis of the “stellar merger scenario” maintaining the same composition and mass of the core of the most massive star (thick lines in Figure 1).

The fact that the second star has already synthesized a large amount of ^4He means that choices need to be made for the envelope composition. Usually, mergers are built assuming that the lowest entropy layers sink to the bottom. However, this would result in a larger He core mass entering the PPI regime and violating the hypothesis of the scenario. Instead, in model “mix” (solid lines in the bottom panel of Figure 1) we fully mix the envelope of the most massive star with the entire second star at merger time. This represents the most favorable scenario preventing growth of the He core, leading to the formation of an He-rich envelope with $X(^4\text{He}) \simeq 0.52$. The total mass in each element is conserved to better than 2%.

As for the opposite limiting case, in model “primordial” (dashed lines in the bottom panel of Figure 1) we ignore the

composition of the second star and increase the envelope mass with the initial composition; that is, with a He abundance of $X(^4\text{He}) \simeq 0.24$. This corresponds to a merger between an evolved primary and a newly formed secondary star with its primordial chemical composition.

4. Post-merger Evolution

We evolve our merger models until the onset of CC. The left panel of Figure 2 shows their post-merger Hertzsprung–Russell (HR) diagram. The evolution proceeds from left toward cooler temperatures. The more He-rich “mix” model has a higher luminosity (L). This can be understood considering that $L \propto \mu^4$ where μ is the mean molecular weight for an ideal gas with constant opacity (e.g., Kippenhahn et al. 2013). Most of the He and carbon core burning happens within the hot S Doradus instability strip (S Dor, gray band in Figure 2), where the star spends 1.9×10^5 years for model “mix” and 8.1×10^4 years for model “primordial.”

Afterward, both evolve into the observationally forbidden region beyond the Humphrey–Davidson (HD) limit (dotted gray line in Figure 2; Humphreys & Davidson 1994). There model “mix” spends its last ~ 3800 years, while the model “primordial” only spends ~ 600 years beyond the HD limit, owing to its lower luminosity.

While both the S Dor strip and the HD limit have been observationally determined at $Z \approx Z_{\odot}$, Davies et al. (2018) recently showed that the empirical HD limit is likely metallicity independent. This might support the theoretical results of Jiang et al. (2018), who found that He opacity is the likely driver of outbursts in luminous stars close to the HD limit and the S Dor strip. Overall, LBVs are known to be at the metallicity of the Small Magellanic Cloud (e.g., Szeifert et al. 1993), and observation of narrow-lined SNe (in particular their isolation relative to other explosions) might be compatible with LBV eruptions happening in more metal-poor parts of galaxies.

The location of our merger models on the HR diagram suggests that they could be affected by envelope instabilities and severe mass loss. The noisiness of the curves is caused by the numerical instabilities, possibly related to physical instabilities in the envelopes (see Section 4.1).

The top-right panel of Figure 2 shows the evolution of the central temperature and density. By construction, both merger models avoid the instability region (gray area) and proceed to CC avoiding pulses. Conversely, a $140 M_{\odot}$ single-star model, hits repeatedly the PI (although off-center; see Renzo et al. 2020a) resulting in large mass loss. The bottom-right panel shows the averaged adiabatic index $\langle \Gamma_1 \rangle$, which stays above the dotted line indicating instability (e.g., Renzo et al. 2020a). Conversely, the averaged adiabatic index of the $140 M_{\odot}$ model drops significantly below $4/3$ repeatedly during PI pulses.

4.1. Estimates for the Continuum-driven Mass Loss

Figure 3 shows the temporal evolution of the ratio of the luminosity L to the Eddington luminosity

$$L_{\text{Edd}} = \frac{4\pi G M c}{\kappa}, \quad (2)$$

where G is the gravitational constant, M the total mass, and c the speed of light. Dashed lines only consider electron-scattering opacity $\kappa \simeq 0.2(1 + X(^1\text{H})) \text{ cm}^2 \text{ g}^{-1}$, while solid

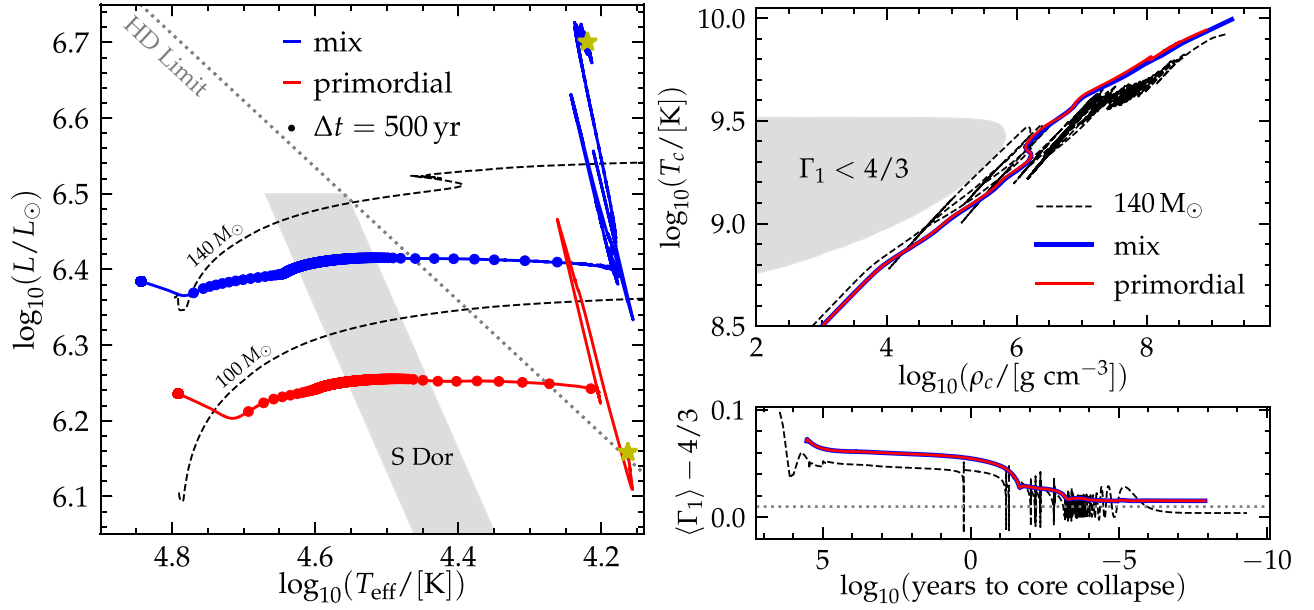


Figure 2. Left panel: HR diagram of the post-merger evolution. Each dot is separated by 500 years. The dashed black lines show for comparison an H-rich $140 M_{\odot}$ star from Renzo et al. (2020a; smaller overshooting, encounters the PPI later), and a $100 M_{\odot}$ model (same overshooting, expected to encounter the PPI). The yellow stars mark the onset of CC. Top-right panel: evolution of the central temperature and density. Bottom-right panel: time evolution of the pressure-weighted average adiabatic index, the star becomes pair-unstable when it drops below the dotted horizontal line (Renzo et al. 2020a).

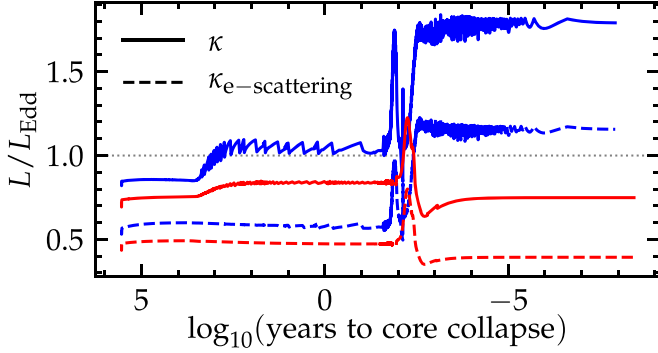


Figure 3. Eddington ratio post-merger as a function of the time left to CC. Solid lines use only the electron-scattering opacity for L_{Edd} , while the dashed lines use the total opacity. The blue (red) lines correspond to the “mix” (“primordial”) merger models. In both cases, the post-merger model exceeds an Eddington ratio of 1 (dashed horizontal line), indicating that eruptive and/or continuum-driven mass loss could occur.

lines correspond to using the stellar surface⁵ opacity in the calculation of the Eddington luminosity.

Both our merger models evolve with high Eddington ratios, and the more luminous and He-rich “mix” model reaches ~ 1 about 1000 years before CC. Again, this suggests that radiatively driven eruptive mass loss might occur even at low metallicity (e.g., Smith 2014). Increasing Z has a large effect over the opacity κ , decreasing L_{Edd} and thus increasing the Eddington ratio. Not surprisingly, preliminary calculations at $Z = 0.02$ with our simple setup proved to be numerically unstable.

Figure 4 shows the internal structure and opacity profile at two selected times for our models. Solid lines correspond to when the models reach an effective temperature $\log_{10}(T_{\text{eff}}/[K]) = 4.5$, roughly in the S Dor instability strip,

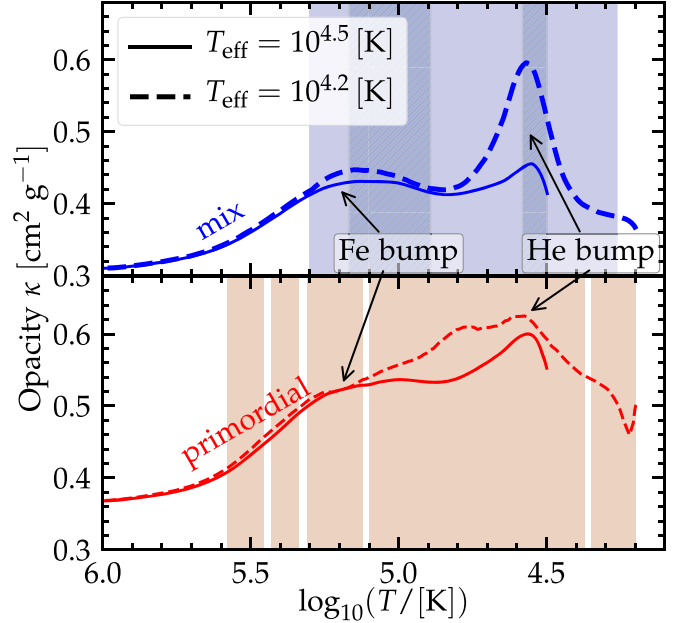


Figure 4. Outer structure of the opacity for two different values of the effective temperature. The top (bottom) panel shows the “mix” (“primordial”) model. The hatched regions indicate convection at $\log_{10}(T_{\text{eff}}/[K]) = 4.5$, with two separate regions in the “mix” model (and none in the “primordial” model). Colored regions mark convective regions at $\log_{10}(T_{\text{eff}}/[K]) = 4.2$.

while dashed lines show models at $\log_{10}(T_{\text{eff}}/[K]) = 4.2$, beyond the HD limit.

While our models have $Z = 2 \times 10^{-4} \simeq Z_{\odot}/100$, two opacity bumps are still evident at both times, one caused by partial recombination of iron (Fe) roughly at $\log_{10}(T/[K]) \simeq 5.3$, and one due to partial He recombination at $\log_{10}(T/[K]) \simeq 4.6$. The presence of these opacity bumps drives inefficient convection layers (shading and hatching in Figure 4). The interplay between density inhomogeneities due to convection and the close-to-super-Eddington luminosity was

⁵ The surface opacity is the average of the Rosseland mean opacity from optical depth $\tau = 2/3$ down to $\tau = 100$.

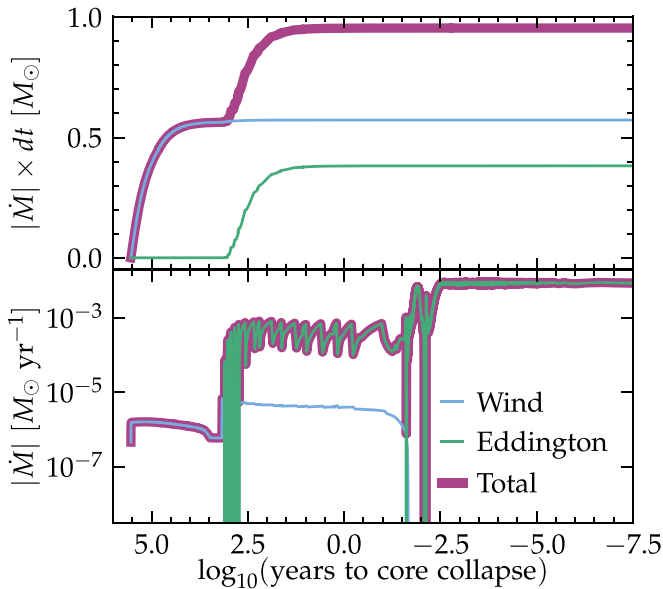


Figure 5. Absolute value of the mass-loss rate (bottom panel) and cumulative mass loss (top panel) as a function of time until CC for our “mix” model.

found to be a key driver of LBV eruptions (at least at $Z = Z_{\odot}$, Jiang et al. 2015, 2018).

Due to insufficient theoretical understanding, our models do not include eruptive LBV-like mass loss or continuum-driven winds in addition to line-driven winds. Nevertheless, following Paxton et al. (2011) and Cantiello et al. (2020) we can estimate the extra mass loss of models exceeding the Eddington luminosity as

$$\dot{M}_{\text{Edd}} \simeq -\frac{L - L_{\text{Edd}}}{v_{\text{esc}}^2}, \quad (3)$$

where L and L_{Edd} are the luminosity and Eddington luminosity, and v_{esc} is the surface escape velocity. We only use this to estimate in post-process the amount of mass that the star would have lost, and we neglect the structural reaction that this may cause (Renzo et al. 2017).

Figure 5 shows the mass-loss rate history (bottom panel) and cumulative mass lost (top panel) for our “mix” model. The wind mass-loss rate (in blue; Vink et al. 2001) removes mass earlier on but becomes subdominant a few hundred years before CC. Then, the Eddington-driven mass loss (green; Equation (3)) becomes dominant. The total mass loss (thick purple) is the sum of the two and is only about $\sim 1 M_{\odot}$, corresponding to a total final mass of $\sim 98 M_{\odot}$. At higher Z more mass loss would be expected. The lower luminosity and Eddington ratio of the “primordial” model result in a smaller mass-loss estimate than for the “mix” model.

5. Discussion and Conclusions

We tested a stellar merger scenario for the production of BHs in the PI mass gap. To avoid the PI regime, this scenario assumes that the core mass of the primary star is unaffected by the merger, with the mass of the secondary fully mixed into the envelope (Di Carlo et al. 2019, 2020a, 2020b; Spera et al. 2019). We do not explore how realistic this assumption is, which needs to be addressed using hydrodynamic calculations (e.g., Lombardi et al. 2002; Glebbeek et al. 2013; Schneider et al. 2019). Standard entropy-sorting post-merger structures

would result in adding the He cores together, which would violate the hypothesis allowing these mergers to avoid the PPI regime.

Assuming that the core does not grow, the envelope of the merger necessarily becomes He-enriched, with the extent of the enrichment depending on when the merger occurs during the main sequence of the secondary star. It could be prevented by allowing the least massive star in the merger to be younger (and less evolved) than the most massive one (e.g., our “primordial” model), so that less He is present in its core. Given the small lifetime differences between very massive stars, this would require not only a non-starburst star formation history, but also fine-tuned timing.

We use detailed stellar evolution calculations to evolve two merger products that assume either an evolved or an unevolved secondary. Because of the He-enrichment, the merger product can be significantly more luminous than a star of similar mass (see Figure 2). It is already possible that most stars with $M \gtrsim 100 M_{\odot}$ will experience large outbursts of mass loss (e.g., Conti 1975), and the He-richness might exacerbate this (Jiang et al. 2018). This suggests that LBV-like outbursts or continuum-driven mass loss can occur even at metallicity as low as $Z = 2 \times 10^{-4} \simeq Z_{\odot}/100$.

We estimated the amount of mass that can be lost by these stellar merger products due to their proximity to the Eddington limit, and found that they can shed up to $\sim 1 M_{\odot}$ during the last few hundred years prior to CC (Section 4.1). This circumstellar material could leave visible imprints in the light curves and spectra of a terminal transient (e.g., Arcavi et al. 2017; Vigna-Gómez et al. 2019), if the final BH formation ejects (a small amount of) mass (e.g., Gilkis & Soker 2014; Quataert et al. 2019).

However, the amount of material lost during the evolution is not large enough to affect the scenario for BH formation in the PI mass gap. We note that stronger mass loss is expected in more metal-rich environment, so that this scenario can only occur below a metallicity threshold. Ultimately, multidimensional radiation hydrodynamical simulations and a better theoretical understanding of LBV eruptions is needed to precisely quantify the pre-collapse mass of these luminous, He-rich merger remnants.

Finally, an estimate of neutrino-driven mass loss (Nadezhin 1980; Lovegrove & Woosley 2013) is required to establish the actual size of the BH formed at CC. The oversized envelopes and He-enrichment keep our merger models relatively blue at the onset of CC ($\log_{10}(T_{\text{eff}}/[\text{K}]) \gtrsim 4.1$); that is, in the intermediate regime where the amount of mass loss at BH formation is unclear (e.g., Fernández et al. 2018). Further studies of the hydrodynamics at merger and at BH formation are needed to assess whether the “stellar merger scenario” can contribute a significant populations of BHs inside the PI SN mass gap.

In the meantime, population synthesis simulations could bracket the range of possibility by considering varying degrees of envelope mass loss before and at CC.

We are thankful to U.N. di Carlo, R. Fernandez, Y. Götzberg, Y. Levin, and N. Smith for helpful exchanges, and to the referee for the prompt and constructive feedback. The Flatiron Institute is supported by the Simons Foundation.

Software: mesaPlot (Farmer 2018), mesaSDK (Townsend 2019), ipython/jupyter (Pérez & Granger 2007),

matplotlib (Hunter 2007), NumPy (van der Walt et al. 2011), MESA(Paxton et al. 2011, 2013, 2015, 2018, 2019).

Appendix MESA Setup

We use MESA version 12778 to compute our models. The MESA equation of state (EOS) is a blend of the OPAL (Rogers & Nayfonov 2002), SCVH (Saumon et al. 1995), PTEH (Pols et al. 1995), HELM (Timmes & Swesty 2000), and PC (Potekhin & Chabrier 2010) EOSs.

Radiative opacities are primarily from OPAL (Iglesias & Rogers 1993, 1996), with low-temperature data from Ferguson et al. (2005) and the high-temperature, Compton-scattering dominated regime by Buchler & Yueh (1976). Electron conduction opacities are from Cassisi et al. (2007).





Nuclear reaction rates are a combination of rates from NACRE (Angulo et al. 1999), JINA REACLIB (Cyburt et al. 2010), plus additional tabulated weak reaction rates (Fuller et al. 1985; Oda et al. 1994; Langanke & Martínez-Pinedo 2000). Screening is included via the prescription of Chugunov et al. (2007). Thermal neutrino loss rates are from Itoh et al. (1996). We compute the pre-merger evolution using an eight-isotope α -chain nuclear reaction network and switch to a 22-isotope nuclear network for the post-merger evolution.

We evolve our models from the pre-main sequence to the terminal-age main sequence of the most massive $58 M_{\odot}$ star, defined as the time when the central hydrogen abundance $X(^1\text{H}) \leq 10^{-4}$. We treat convection using the Ledoux criterion, and include thermohaline mixing (until the central temperature $\log_{10}(T_c/[\text{K}]) > 9.45$; Farmer et al. 2016) and semiconvection, both with an efficiency factor of 1. We assume $\alpha_{\text{MLT}} = 2.0$ and use Brott et al. (2011) overshooting for the convective core burning. We have tested that varying core overshooting does not impact significantly the post-merger evolution; however, when including shell overshooting and/or undershooting we were unable to find solutions to the stellar structure equations. Moreover, we employ the MLT++ artificial enhancement of the convective flux (e.g., Paxton et al. 2015; Jiang et al. 2015). Stellar winds are included using the algorithms from Vink et al. (2001) with an efficiency factor of 1.

To compute through the very late phases, we reduce the core resolution and increase the numerical solver tolerance when the central temperature increases above $\log_{10}(T_c/[\text{K}]) > 9.45$. We define the onset of CC when the iron-core infall velocity exceeds 1000 km s^{-1} (e.g., Woosley et al. 2002).

The inlists, processing scripts, and model output will be made available at [10.5281/zenodo.4062493](https://doi.org/10.5281/zenodo.4062493).

ORCID iDs

M. Renzo  <https://orcid.org/0000-0002-6718-9472>
M. Cantiello  <https://orcid.org/0000-0002-8171-8596>
B. D. Metzger  <https://orcid.org/0000-0002-4670-7509>
Y.-F. Jiang
(姜燕飞)  <https://orcid.org/0000-0002-2624-3399>

References

- Abbott, R., Abbott, T. D., Abraham, S., et al. 2020a, arXiv:2009.01075
Abbott, R., Abbott, T. D., Abraham, S., et al. 2020b, arXiv:2009.01190
Aghakhanloo, M., Murphy, J. W., Smith, N., & Hložek, R. 2017, *MNRAS*, **472**, 591
Angulo, C., Arnould, M., Rayet, M., et al. 1999, *NuPhA*, **656**, 3
Arcavi, I., Howell, D. A., Kasen, D., et al. 2017, *Natur*, **551**, 210
Barkat, Z., Rakavy, G., & Sack, N. 1967, *PhRvL*, **18**, 379
Bartos, I., Kocsis, B., Haiman, Z., & Márka, S. 2017, *ApJ*, **835**, 165
Belczynski, K. 2020, arXiv:2009.13526
Belczynski, K., Hirschi, R., Kaiser, E. A., et al. 2020, *ApJ*, **890**, 113
Brott, I., de Mink, S. E., Cantiello, M., et al. 2011, *A&A*, **530**, A115
Buchler, J. R., & Yueh, W. R. 1976, *ApJ*, **210**, 440
Cantiello, M., Jermyn, A. S., & Lin, D. N. C. 2020, arXiv:2009.03936
Cassisi, S., Potekhin, A. Y., Pietrinferni, A., Catelan, M., & Salaris, M. 2007, *ApJ*, **661**, 1094
Chugunov, A. I., Dewitt, H. E., & Yakovlev, D. G. 2007, *PhRvD*, **76**, 025028
Conti, P. S. 1975, *MSRSL*, **9**, 193
Croon, D., McDermott, S. D., & Sakstein, J. 2020a, arXiv:2007.07889
Croon, D., McDermott, S. D., & Sakstein, J. 2020b, arXiv:2007.00650
Cyburt, R. H., Amthor, A. M., Ferguson, R., et al. 2010, *ApJS*, **189**, 240
Davies, B., Crowther, P. A., & Beasor, E. R. 2018, *MNRAS*, **478**, 3138
De Luca, V., Desjacques, V., Franciolini, G., Pani, P., & Riotto, A. 2020, arXiv:2009.01728
de Mink, S. E., Langer, N., Izzard, R. G., Sana, H., & de Koter, A. 2013, *ApJ*, **764**, 166
Di Carlo, U. N., Giacobbo, N., Mapelli, M., et al. 2019, *MNRAS*, **487**, 2947
Di Carlo, U. N., Mapelli, M., Bouffanaïs, Y., et al. 2020a, *MNRAS*, **497**, 1043
Di Carlo, U. N., Mapelli, M., Giacobbo, N., et al. 2020b, *MNRAS*, **498**, 495
Farmer, R. 2018, *rjfarmer/mesaplot*, v1.0.6, Zenodo, doi:10.5281/zenodo.1441329
Farmer, R., Fields, C. E., Petermann, I., et al. 2016, *ApJS*, **227**, 22
Farmer, R., Renzo, M., de Mink, S., Fishbach, M., & Justham, S. 2020, arXiv:2006.06678
Farmer, R., Renzo, M., de Mink, S. E., Marchant, P., & Justham, S. 2019, *ApJ*, **887**, 53
Farrell, E. J., Groh, J. H., Hirschi, R., et al. 2020, arXiv:2009.06585
Ferguson, J. W., Alexander, D. R., Allard, F., et al. 2005, *ApJ*, **623**, 585
Fernández, R., Quataert, E., Kashiya, K., & Coughlin, E. R. 2018, *MNRAS*, **476**, 2366
Fishbach, M., & Holz, D. E. 2020, arXiv:2009.05472
Fragione, G., Grishin, E., Leigh, N. W. C., Perets, H. B., & Perna, R. 2019, *MNRAS*, **488**, 47
Fragione, G., Loeb, A., & Rasio, F. A. 2020, arXiv:2009.05065
Fuller, G. M., Fowler, W. A., & Newman, M. J. 1985, *ApJ*, **293**, 1
Gaburov, E., Lombardi, J. C., & Portegies Zwart, S. 2008, *MNRAS*, **383**, L5
Gilks, A., & Soker, N. 2014, *MNRAS*, **439**, 4011
Glebbeek, E., Gaburov, E., Portegies Zwart, S., & Pols, O. R. 2013, *MNRAS*, **434**, 3497
Heger, A., Langer, N., & Woosley, S. E. 2000, *ApJ*, **528**, 368
Humphreys, R. M., & Davidson, K. 1994, *PASP*, **106**, 1025
Hunter, J. D. 2007, *CSE*, **9**, 90
Iglesias, C. A., & Rogers, F. J. 1993, *ApJ*, **412**, 752
Iglesias, C. A., & Rogers, F. J. 1996, *ApJ*, **464**, 943
Itoh, N., Hayashi, H., Nishikawa, A., & Kohyama, Y. 1996, *ApJS*, **102**, 411
Jiang, Y.-F., Cantiello, M., Bildsten, L., et al. 2018, *Natur*, **561**, 498
Jiang, Y.-F., Cantiello, M., Bildsten, L., Quataert, E., & Blaes, O. 2015, *ApJ*, **813**, 74
Justham, S., Podsiadlowski, P., & Vink, J. S. 2014, *ApJ*, **796**, 121
Kinugawa, T., Nakamura, T., & Nakano, H. 2020, arXiv:2009.06922
Kippenhahn, R., Weigert, A., & Weiss, A. 2013, *Stellar Structure and Evolution* (Berlin: Springer)
Kremer, K., Spera, M., Becker, D., et al. 2020, arXiv:2006.10771
Langanke, K., & Martínez-Pinedo, G. 2000, *NuPhA*, **673**, 481
Langer, N. 1998, *A&A*, **329**, 551
Leung, S.-C., Nomoto, K., & Blinnikov, S. 2019, *ApJ*, **887**, 72
Lombardi, J. C., Jr., Warren, J. S., Rasio, F. A., Sills, A., & Warren, A. R. 2002, *ApJ*, **568**, 939
Lovegrove, E., & Woosley, S. E. 2013, *ApJ*, **769**, 109
Maeder, A., & Meynet, G. 2000, *ARA&A*, **38**, 143
Mapelli, M., Santoliquido, F., Bouffanaïs, Y., et al. 2020, arXiv:2007.15022
Marchant, P., & Moriya, T. J. 2020, *A&A*, **640**, L18
Marchant, P., Renzo, M., Farmer, R., et al. 2019, *ApJ*, **882**, 36
McKernan, B., Ford, K. E. S., Kocsis, B., Lyra, W., & Winter, L. M. 2014, *MNRAS*, **441**, 900
McKernan, B., Ford, K. E. S., Lyra, W., & Perets, H. B. 2012, *MNRAS*, **425**, 460
Menon, A., & Heger, A. 2017, *MNRAS*, **469**, 4649
Morozova, V., Piro, A. L., Renzo, M., et al. 2015, *ApJ*, **814**, 63
Nadezhin, D. K. 1980, *Ap&SS*, **69**, 115
Oda, T., Hino, M., Muto, K., Takahara, M., & Sato, K. 1994, *ADNDT*, **56**, 231
Paxton, B., Bildsten, L., Dotter, A., et al. 2011, *ApJS*, **192**, 3
Paxton, B., Cantiello, M., Arras, P., et al. 2013, *ApJS*, **208**, 4

- Paxton, B., Marchant, P., Schwab, J., et al. 2015, [ApJS](#), **220**, 15
- Paxton, B., Schwab, J., Bauer, E. B., et al. 2018, [ApJS](#), **234**, 34
- Paxton, B., Smolec, R., Schwab, J., et al. 2019, [ApJS](#), **243**, 10
- Pérez, F., & Granger, B. E. 2007, [CSE](#), **9**, 21
- Perna, R., Lazzati, D., & Cantiello, M. 2018, [ApJ](#), **859**, 48
- Perna, R., Wang, Y.-H., Farr, W. M., Leigh, N., & Cantiello, M. 2019, [ApJL](#), **878**, L1
- Podsiadlowski, P. 1992, [PASP](#), **104**, 717
- Pols, O. R., Tout, C. A., Eggleton, P. P., & Han, Z. 1995, [MNRAS](#), **274**, 964
- Potekhin, A. Y., & Chabrier, G. 2010, [CoPP](#), **50**, 82
- Quataert, E., Lecoanet, D., & Coughlin, E. R. 2019, [MNRAS](#), **485**, L83
- Renzo, M., Farmer, R., Justham, S., et al. 2020a, [A&A](#), **640**, A56
- Renzo, M., Farmer, R. J., Justham, S., et al. 2020b, [MNRAS](#), **493**, 4333
- Renzo, M., Ott, C. D., Shore, S. N., & de Mink, S. E. 2017, [A&A](#), **603**, A118
- Rodríguez, C. L., Kremer, K., Grudić, M. Y., et al. 2020, [ApJL](#), **896**, L10
- Rogers, F. J., & Nayfonov, A. 2002, [ApJ](#), **576**, 1064
- Roupas, Z., & Kazanas, D. 2019, [A&A](#), **621**, L1
- Safarzadeh, M., & Haiman, Z. 2020, [arXiv:2009.09320](#)
- Sakstein, J., Croon, D., McDermott, S. D., Straight, M. C., & Baxter, E. J. 2020, [arXiv:2009.01213](#)
- Saumon, D., Chabrier, G., & van Horn, H. M. 1995, [ApJS](#), **99**, 713
- Schneider, F. R. N., Ohlmann, S. T., Podsiadlowski, P., et al. 2019, [Natur](#), **574**, 211
- Smith, N. 2014, [ARA&A](#), **52**, 487
- Spera, M., Mapelli, M., Giacobbo, N., et al. 2019, [MNRAS](#), **485**, 889
- Stone, N. C., Metzger, B. D., & Haiman, Z. 2017, [MNRAS](#), **464**, 946
- Szeifert, T., Stahl, O., Wolf, B., et al. 1993, [A&A](#), **280**, 508
- Timmes, F. X., & Swesty, F. D. 2000, [ApJS](#), **126**, 501
- Townsend, R. 2019, MESA SDK for Linux, 20190911
- van der Walt, S., Colbert, S. C., & Varoquaux, G. 2011, [CSE](#), **13**, 22
- van Son, L. A. C., De Mink, S. E., Broekgaarden, F. S., et al. 2020, [ApJ](#), **897**, 100
- Vigna-Gómez, A., Justham, S., Mandel, I., de Mink, S. E., & Podsiadlowski, P. 2019, [ApJL](#), **876**, L29
- Vink, J. S., de Koter, A., & Lamers, H. J. G. L. M. 2001, [A&A](#), **369**, 574
- Woosley, S. E. 2017, [ApJ](#), **836**, 244
- Woosley, S. E., Heger, A., & Weaver, T. A. 2002, [RvMP](#), **74**, 1015
- Zhao, X., & Fuller, J. 2020, [MNRAS](#), **495**, 249